Nr. 12
10. March 2014

Leopold-Franzens-Universität Innsbruck

Preprint-Series: Department of Mathematics - Applied Mathematics

Recovering a function from circular means or wave data on the boundary of parabolic domains

Markus Haltmeier and Sergiy Pereverzev Jr.

Technikerstraße 21a - 6020 Innsbruck - Austria
Tel.: +43 512 507 53803 Fax: +43 512 507 53898
https://www.applied-math.uibk.ac.at

Recovering a function from circular means or wave data on the boundary of parabolic domains

Markus Haltmeier and Sergiy Pereverzyev Jr.

Department of Mathematics
University of Innsbruck
Technikestraße 21a, A-6020 Innsbruck
E-mail: markus.haltmeier,sergiy.pereverzyev@uibk.ac.at

March 8, 2014

Abstract

Determining a function from its circular means with restricted centers is crucial for many modern medical imaging and remote sensing applications. Examples include photo- and thermoacoustic tomography, ultrasound imaging, and synthetic aperture radar. In this paper we derive an explicit inversion formula for the case where the centers of the circles of integration are restricted to the boundary of parabolic domains. A similar result is obtained for recovering the initial data of the wave equation from data on the boundary of a parabolic domain.

1 Introduction

Let $\Omega \subset \mathbb{R}^2$ be a domain in the plane with a smooth boundary $\partial\Omega$. We write $C_c^\infty(\Omega)$ for the set of all smooth functions $f\colon \mathbb{R}^2 \to \mathbb{R}$ which are compactly supported in Ω. In this paper, we study the problem of recovering an unknown function $f \in C_c^\infty(\Omega)$ from either its circular means or the solution of the wave equation given on the boundary of Ω. We are in particular interested in the situation where Ω is a parabolic domain.

We denote the circular means of a function $f \in C_c^\infty(\Omega)$ by

$$(\mathcal{M}f)(x,r) := \frac{1}{2\pi r} \int_{\partial B(x,r)} f(y)\, \mathrm{d}s(y), \qquad \text{for } (x,r) \in \mathbb{R}^2 \times (0,\infty),$$

where $\mathrm{d}s$ denotes the usual arc length measure and $\partial B(x,r) := \{y \in \mathbb{R}^2 \mid |x-y| = r\}$ a circle of radius r centered at x with respect to the usual Euclidian norm. Further, we write $\mathcal{U}f\colon \mathbb{R}^2 \times (0,\infty) \to \mathbb{R}$ for the solution of the following initial value problem for the wave equation,

$$\begin{cases} (\partial_t^2 - \Delta_x)\, u(x,t) = 0 & \text{for } (x,t) \in \mathbb{R}^2 \times (0,\infty) \\ u(x,0) = f(x) & \text{for } x \in \mathbb{R}^2 \\ (\partial_t u)(x,0) = 0 & \text{for } x \in \mathbb{R}^2\,. \end{cases}$$

With this notations, the reconstruction problems under study consist in recovering the unknown function $f \in C_c^\infty(\Omega)$ from either its circular means

$$m(x,r) = (\mathcal{M}f)(x,r) \quad \text{for } (x,r) \in \partial\Omega \times (0,\infty), \tag{1.1}$$

or the corresponding wave boundary data

$$u(x,t) = (\mathcal{U}f)(x,t) \quad \text{for } (x,t) \in \partial\Omega \times (0,\infty). \tag{1.2}$$

Since the operator $\mathcal{U}$ can be expressed in terms of the operator $\mathcal{M}$, and vice versa, the problems (1.1) and (1.2) are basically equivalent.

Both reconstruction problems (1.1) and (1.2) are essential for the so-called photoacoustic tomography (PAT) and thermoacoustic tomography (TAT), which are novel hybrid imaging methods. In the standard setting of PAT/TAT, where so-called point-like detectors are used, these problems arise for three spatial dimensions [28, 16]. The two-dimensional version, which we consider in this paper, arises in PAT/TAT with so-called linear integrating detectors [5, 26]. Problems (1.1) and (1.2) are also relevant for other imaging methods, such as SONAR [1] or ultrasound tomography [23].

1.1 Explicit reconstruction formulas

The reconstruction problems (1.1) and (1.2) can be approached by various solution techniques, such as time reversal [6, 15], Fourier domain algorithms [10, 14, 30], and algorithms based on explicit reconstruction formulas of the back-projection type [1, 7, 9, 8, 11, 17, 19, 22]. Among these techniques, the derivation of the explicit reconstruction formulas of the back-projection type is particularly appealing. Such formulas consist of explicitly given operators $\mathcal{F}$, $\mathcal{G}$ that recover the function f from the data m or u respectively. Explicit reconstruction formulas have a number of attractive features. For example, they allow an analytical study of the influence of the measurement and modeling errors in the data m or u. Further, the numerical implementation of explicitly given reconstruction formulas is often quite straightforward and allows the derivation of efficient algorithms for recovering the unknown function.

However, explicit inversion formulas are currently known only for special domains. For example, they are known for spheres, cylinders, and hyperplanes. Recently, explicit inversion formulas for elliptical domains have been found in several works, see [2, 12, 13, 21, 24]. In this paper, we show that the formulas of [12] provide exact recovery of the function f also for data on the boundaries of parabolic domains.

1.2 Statement of the main results

For a domain $\Omega \subset \mathbb{R}^2$, given data $m, u\colon \partial\Omega \times (0,\infty) \to \mathbb{R}$, and a reconstruction point $x_0 \in \Omega$ consider the following reconstruction integrals

$$\mathcal{F}(\partial\Omega, m, x_0) = \frac{1}{\pi} \int_{\partial\Omega} \langle \nu_x, x_0 - x \rangle \int_0^\infty \frac{\partial_r m(x,r)}{r^2 - |x - x_0|^2} \, \mathrm{d}r \mathrm{d}s(x), \tag{1.3}$$

$$\mathcal{G}(\partial\Omega, u, x_0) = \frac{1}{\pi} \int_{\partial\Omega} \langle \nu_x, x_0 - x \rangle \int_{|x_0 - x|}^{\infty} \frac{\left(\partial_t t^{-1} u\right)(x,t)}{\sqrt{t^2 - |x - x_0|^2}} \, \mathrm{d}t\mathrm{d}s(x) \,. \tag{1.4}$$

In these formulas, ν_x denotes the outward pointing unit normal to $\partial\Omega$ at the point $x \in \partial\Omega$, and the inner integral in (1.3) is understood in the principal value sense.

In [12] it has been shown that for any elliptical domain the formulas $\mathcal{F}$ and $\mathcal{G}$ exactly recover any smooth function f with compact support in an elliptical domain Ω from data $m = \mathcal{M}f$ and $u = \mathcal{U}f$, respectively. In the present work we will show, that the same results also hold for parabolic domains $\Omega = \mathcal{P}$, which are domains that are bounded by a parabola. After translation and rotation we may assume that the parabolic domain has the form

$$\mathcal{P} = \left\{ (a, b) \in \mathbb{R}^2 \mid b > ca^2 \right\} \qquad \text{for some constant } c > 0 \,. \tag{1.5}$$

More precisely we will prove the following theorems:

Theorem 1.1 (Recovery from circular means)**.** *Let $\mathcal{P}$ be a parabolic domain as in (1.5) and suppose $f \in C_c^\infty(\mathcal{P})$. Then, for every reconstruction point $x_0 \in \mathcal{P}$, we have*

$$\begin{aligned} f(x_0) &= \mathcal{F}(\partial\mathcal{P}, \mathcal{M}f, x_0) \\ &= \frac{1}{\pi} \int_{\partial\mathcal{P}} \langle \nu_x, x_0 - x \rangle \int_0^{\infty} \frac{\partial_r \mathcal{M}f(x,r)}{r^2 - |x - x_0|^2} \, \mathrm{d}r\mathrm{d}s(x) \,. \end{aligned} \tag{1.6}$$

Proof. See Section 3.1. □

Theorem 1.2 (Recovery from wave data)**.** *Let $\mathcal{P}$ be a parabolic domain as in (1.5) and suppose $f \in C_c^\infty(\mathcal{P})$. Then, for every reconstruction point $x_0 \in \mathcal{P}$, we have*

$$\begin{aligned} f(x_0) &= \mathcal{G}(\partial\mathcal{P}, \mathcal{U}f, x_0) \\ &= \frac{1}{\pi} \int_{\partial\mathcal{P}} \langle \nu_x, x_0 - x \rangle \int_{|x - x_0|}^{\infty} \frac{\left(\partial_t t^{-1} \mathcal{U}f\right)(x,t)}{\sqrt{t^2 - |x - x_0|^2}} \, \mathrm{d}t\mathrm{d}s(x) \,. \end{aligned} \tag{1.7}$$

Proof. See Section 3.2. □

As we will show, it is sufficient to prove the reconstruction formula (1.6). The reconstruction formula (1.7) will then follow quickly from the relationships between the operators defined in (1.3), (1.4). The proof of formula (1.6) presented below is based on the corresponding formula of [12] for data on the boundary of ellipses and the fact that any parabola can be obtained as the pointwise limit of a sequence of ellipses.

1.3 Organization of the paper

The paper is organized as follows. In Section 2, we derive auxiliary results that we require for the proofs of Theorems 1.1 and 1.2. In particular, we derive an equivalent

expression of the operator $\mathcal{F}$ that will be more convenient for our further analysis. Further, we will study the approximation of parabolic domains by elliptical domains. The proofs of Theorems 1.1 and 1.2 will finally be presented in Section 3. In Section 4, we show the results of the numerical realization of the formula (1.4) for the parabolic and several related domains. We finish the paper with some concluding remarks in Section 5.

2 Auxiliary results

In this section we derive auxiliary lemmas that will be used for the proof of our main results. The first auxiliary result is an alternative representation of the inversion integral (1.3) and will be stated in Proposition 2.1. The second auxiliary result concerns the approximation of parabolas by elliptical domains; see Proposition 2.3.

2.1 Alternative representations of $\mathcal{F}$

We derive equivalent expressions for (1.3) by rewriting the outer integral in (1.3) as an integral over the unit circle. For that purpose, we construct a special parameterization $\Phi\colon S^1 \to \partial\Omega$ depending on the reconstruction point $x_0 \in \Omega$. Consider the mapping $\Psi\colon \partial\Omega \to S^1\colon x \mapsto (x - x_0)/|x - x_0|$. If Ω is convex and bounded, then Ψ is bijective and therefore invertible. The inverse function

$$\Phi\colon S^1 \to \partial\Omega\colon \omega \mapsto \Psi^{-1}(\omega) \tag{2.1}$$

is taken as the aforementioned parameterization. This parameterization is illustrated in Figure 1 and will be referred to as the circular parameterization of $\partial\Omega$ around the center x_0.

Using the circular parameterization of $\partial\Omega$, the formulas (1.3) and (1.4) can be written in equivalent forms involving integrals over the unit circle. In the case of formula (1.3) this yields the following result.

Proposition 2.1. *Let $\Omega \subset \mathbb{R}^2$ be a convex bounded domain, $f \in C_c^\infty(\Omega)$, and $x_0 \in \Omega$ be any reconstruction point. Set $m = \mathcal{M}f$. Then, with the circular parameterization Φ defined in (2.1), and with $\mathrm{d}\omega$ denoting the arc length measure on S^1, the following assertions hold true:*

(a) We have

$$\mathcal{F}(\partial\Omega, m, x_0) = -\frac{1}{\pi}\int_{S^1} |\Phi(\omega) - x_0|^2 \int_0^\infty \frac{\partial_r m\,(\Phi(\omega), r)}{r^2 - |\Phi(\omega) - x_0|^2}\,\mathrm{d}r\mathrm{d}\omega\,. \tag{2.2}$$

(b) There exists a bounded interval $I \subset \mathbb{R}$ depending only on the support of f but neither on Ω nor on x_0, such that

$$\mathcal{F}(\partial\Omega, m, x_0) = \frac{1}{2\pi}\int_{S^1}\int_I |\Phi(\omega) - x_0|\,\partial_r^2 m\,(\Phi(\omega), \rho + |\Phi(\omega) - x_0|)\ln|\rho|\,\mathrm{d}\rho\mathrm{d}\omega$$

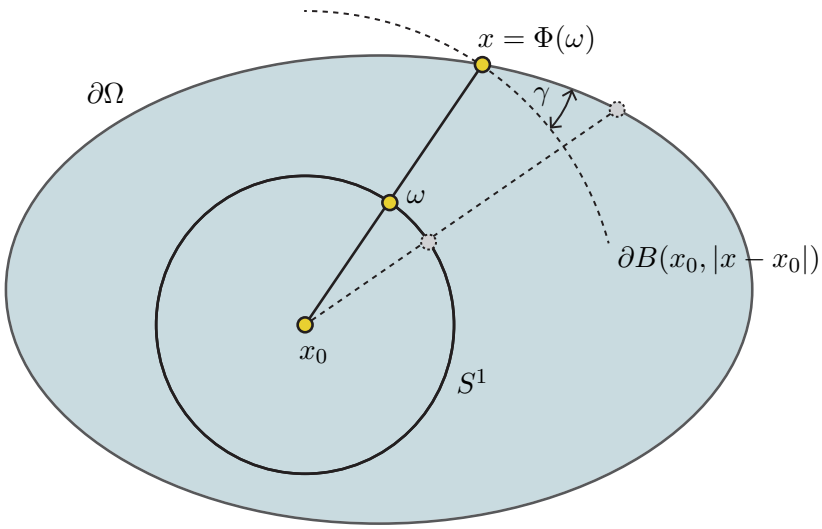

Figure 1: **Circular Parameterization of $\partial\Omega$.** Any point on the boundary can be uniquely be written in the form $x = \Phi(\omega) = |x - x_0|\,\omega$ for a unique $\omega \in S^1$. We have $|x - x_0|\,\mathrm{d}\omega = \mathrm{d}s(x)\cos(\gamma)$, where γ is the angle between $\partial\Omega$ and the circle $\partial B(x_0, |x - x_0|)$ of radius $|x - x_0|$ centered at x_0. We also have that $\langle \nu_x, x - x_0\rangle = |x - x_0|\cos(\gamma)$ (see Figure 2), and therefore $|x - x_0|^2\,\mathrm{d}\omega = \langle \nu_x, x - x_0\rangle\,\mathrm{d}s(x)$.

$$+\frac{1}{2\pi}\int_{S^1}\int_I \frac{|\Phi(\omega) - x_0|}{\rho + 2\,|\Phi(\omega) - x_0|}\,\partial_r m\left(\Phi(\omega), \rho + |\Phi(\omega) - x_0|\right)\,\mathrm{d}\rho\mathrm{d}\omega\,. \quad (2.3)$$

Here we have set $m(\,\cdot\,, r) := 0$ for $r \le 0$.

Proof. (a) By the transformation rule using the parameterization (2.1), for any integrable function $g\colon \partial\Omega \to \mathbb{R}$ we have

$$\int_{\partial\Omega} g(x)\,\langle \nu_x, x - x_0\rangle\,\mathrm{d}s(x) = \int_{S^1} |\Phi(\omega) - x_0|^2 g\left(\Phi(\omega)\right)\,\mathrm{d}\omega\,. \quad (2.4)$$

Here we used the identity $\langle \nu_x, x - x_0\rangle\,\mathrm{d}s(x) = |x - x_0|^2\,\mathrm{d}\omega$; see Figures 1 and 2. Application of (2.4) to the outer integral in (1.3) yields (2.2).

(b) To proof the second formula, we first note that

$$\frac{1}{r^2 - |\Phi(\omega) - x_0|^2} = \frac{1}{2|\Phi(\omega) - x_0|}\left(\frac{1}{r - |\Phi(\omega) - x_0|} - \frac{1}{r + |\Phi(\omega) - x_0|}\right).$$

Thus, (2.2) yields

$$\begin{aligned} 2\pi\mathcal{F}(\partial\Omega, m, x_0) = &-\int_{S^1} |\Phi(\omega) - x_0| \int_0^\infty \frac{\partial_r m\left(\Phi(\omega), r\right)}{r - |\Phi(\omega) - x_0|}\,\mathrm{d}r\,\mathrm{d}\omega \\ &+\int_{S^1} |\Phi(\omega) - x_0| \int_0^\infty \frac{\partial_r m\left(\Phi(\omega), r\right)}{r + |\Phi(\omega) - x_0|}\,\mathrm{d}r\,\mathrm{d}\omega\,. \end{aligned}$$

Recalling that the P.V. $\left(\frac{1}{r}\right)$ is the distributional derivative of $\log|r|$ and performing one integration by parts in the first integral of the last displayed equation, we see

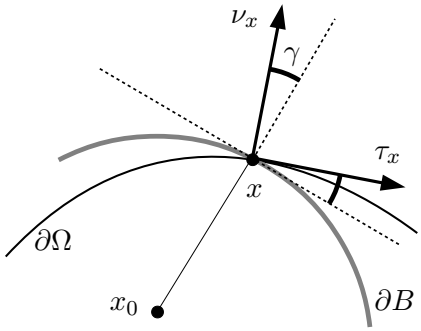

Figure 2: The angle γ between the tangents of $\partial\Omega$ and the circle $\partial B(x_0, |x - x_0|)$ is equal to the angle between the unit normal ν_x and $x - x_0$. Therefore, $\langle \nu_x, x - x_0 \rangle = |x - x_0| \cos(\gamma)$.

that $2\pi\mathcal{F}(\partial\Omega, m, x_0)$ can further be written as

$$\int_{S^1} |\Phi(\omega) - x_0| \int_0^\infty \partial_r^2 m\left(\Phi(\omega), r\right) \ln\left(|r - |\Phi(\omega) - x_0||\right) \,\mathrm{d}r \,\mathrm{d}\omega \\ + \int_{S^1} |\Phi(\omega) - x_0| \int_0^\infty \frac{\partial_r m\left(\Phi(\omega), r\right)}{r + |\Phi(\omega) - x_0|} \,\mathrm{d}r\mathrm{d}\omega \,.$$

Next, we make the following change of variables $\rho := r - |\Phi(\omega) - x_0|$ in both integrals. Due to the compact support of f, the values of ρ may be restricted to a finite interval I independent of ω and x_0. The last displayed equation therefore yields

$$2\pi\mathcal{F}(\partial\Omega, m, x_0) = \int_{S^1} \int_I |\Phi(\omega) - x_0| \, \partial_r^2 m\left(\Phi(\omega), \rho + |\Phi(\omega) - x_0|\right) \ln|\rho| \,\mathrm{d}\rho\mathrm{d}\omega \\ + \int_{S^1} \int_I |\Phi(\omega) - x_0| \, \frac{\partial_r m\left(\Phi(\omega), \rho + |\Phi(\omega) - x_0|\right)}{\rho + 2\,|\Phi(\omega) - x_0|} \,\mathrm{d}\rho\mathrm{d}\omega \,.$$

This is the desired identity (2.3). □

Remark 2.2 (Proposition 2.1 for parabolic domains). For a parabolic domain $\mathcal{P}$ as in (1.5), which is convex but unbounded, the image of the function Ψ does not contain $e_2 = (0, 1)$, which is the element in S^1 being parallel to the axis of symmetry of the parabola and pointing away from its vertex. Consequently, the corresponding circular parameterization $\Phi\colon S^1 \setminus \{e_2\} \to \partial\mathcal{P}$ is only defined for $\omega \neq e_2$. Because $\{e_2\}$ is a set of measure zero, (2.4) as well as the identities (2.2) and (2.3) in Proposition 2.1 also hold true for parabolic domains $\Omega = \mathcal{P}$.

2.2 Approximation of a parabola by ellipsoids

As already mentioned in the introduction, any parabola can be obtained as the pointwise limit of a sequence of ellipses. A precise statement of this fact is given in the following proposition.

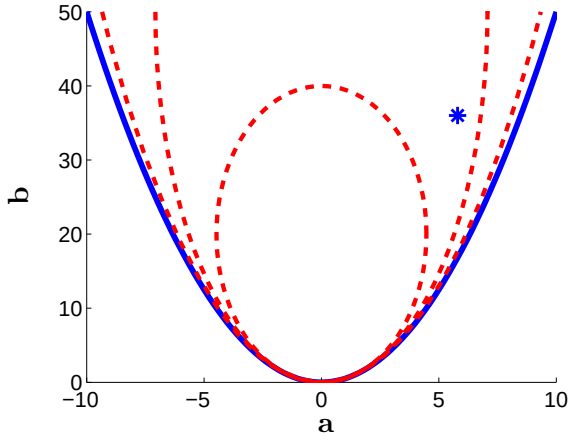

Figure 3: Elliptical boundaries $\partial\mathcal{E}_n$ for $n = 20, 50, 200$ (dashed red curves), parabolic boundary $\partial\mathcal{P}$ (solid blue curve), and a point $x_0 \in \mathcal{P}$ (asterisk). The picture illustrates that $\partial\mathcal{E}_n$ converges pointwise to $\partial\mathcal{P}$ such that (2.5) holds. Also, for the chosen point x_0, we have that $x_0 \in \mathcal{E}_n$ for $n \geq 50$.

Proposition 2.3. *Let $\mathcal{P} \subset \mathbb{R}^2$ be a parabolic domain as in (1.5). Then, for every compact subset $K \subset \mathcal{P}$ and every $x_0 \in K$, there exists a sequence $(\mathcal{E}_n)_{n\in\mathbb{N}}$ of elliptical domains $\mathcal{E}_n \subset \mathbb{R}^2$ such that the following hold:*

(a) We have $K \subset \mathcal{E}_n$ for all $n \in \mathbb{N}$.

(b) Let Φ_n denote the circular parameterization of $\partial\mathcal{E}_n$ around x_0. Then

$$\lim_{n\to\infty} \Phi_n(\omega) = \Phi(\omega) \quad \text{for all } \omega \in S^1 \setminus \{e_2\} \,. \tag{2.5}$$

Proof. Let us take a sequence of ellipses where one focus and the the semi-latus rectum are kept fixed, and the other focus moves arbitrarily far away. Any parabola can be be written as the point-wise limit of such a sequence of ellipses. Below we shall verify this for the parabola

$$\partial\mathcal{P} = \left\{ (a,b) \in \mathbb{R}^2 \;\middle|\; b = \frac{a^2}{2} \right\}.$$

The general case then follows after affine scaling.

To that end, consider the following sequence of ellipses with the fixed focus $(0, 1/2) \in \mathbb{R}^2$ and semi-latus rectum 1 defined by

$$\partial\mathcal{E}_n = \left\{ (a,b) \in \mathbb{R}^2 \;\middle|\; \frac{a^2}{n} + \frac{(b-T_n)^2}{n^2} = 1 \right\} \quad \text{with} \quad T_n := \frac{1}{2} + \sqrt{n^2 - n}\,,$$

see Figure 3.

Now fix any $a \in \mathbb{R}$. Then for every $n \in \mathbb{N}$ there is a unique $b_n \in (0, T_n)$ such that $(a, b_n) \in \partial\mathcal{E}_n$. We have $a^2/n + (b_n - T_n)^2/n^2 = 1$, and therefore

$$b_n = T_n - \sqrt{n^2 - na^2} = \frac{1}{2} + \sqrt{n^2 - n} - \sqrt{n^2 - na^2}$$
$$= \frac{1}{2} + \frac{a^2 - 1}{\sqrt{1 - 1/n} + \sqrt{1 - a^2/n}} \longrightarrow \frac{a^2}{2} \qquad \text{as } n \to \infty\,.$$

This, in particular, shows that for every compact subset $K \subset \mathcal{P}$, there exists $n_0 \in \mathbb{N}$ such that $K \subset \mathcal{E}_n$ for all $n \geq n_0$. Replacing $\mathcal{E}_n$ by $\mathcal{E}_{n-n_0}$ yields a sequence of ellipses $\mathcal{E}_n$ containing K. Further, the last displayed equation shows that for any $\omega \neq (0,1)$, the circular parameterisations $\Phi_n(\omega)$ of $\partial\mathcal{E}_n$ point-wise converge to the circular parameterisation $\Phi(\omega)$ of $\partial\mathcal{P}$. □

3 Proofs of main results

Throughout this section, let $\mathcal{P}$ be a parabolic domain as in (1.5) and suppose $f \in C_c^\infty(\mathcal{P})$. Further, for a given reconstruction point $x_0 \in \mathcal{P}$ in the parabolic domain consider the circular parameterisation $\Phi\colon S^1 \to \partial\mathcal{P} \setminus \{e_2\}$.

According to Proposition 2.3 applied with $K = \{x_0\} \cup \operatorname{supp}(f)$, we may choose a sequence of elliptical domains $\mathcal{E}_n$, such that $x_0 \in \mathcal{E}_n$, $\operatorname{supp}(f) \subset \mathcal{E}_n$ for all $n \in \mathbb{N}$ and

$$\lim_{n\to\infty} \Phi_n(\omega) = \Phi(\omega) \qquad \text{pointwise for all } \omega \in S^1 \setminus \{e_2\}\,,$$

where $\Phi_n\colon S^1 \to \partial\mathcal{E}_n$ is the circular parameterization of $\partial\mathcal{E}_n$ around x_0.

3.1 Proof of Theorem 1.1

According to [12] the inversion integral (1.3) exactly recovers f for any ellipsoid $\mathcal{E}_n$. Together with Proposition 2.1 this shows

$$2\pi f(x) = \int_{S^1}\int_I |\Phi_n(\omega) - x_0| \left(\partial_r^2 \mathcal{M}f\right)(\Phi_n(\omega), \rho + |\Phi_n(\omega) - x_0|) \ln|\rho|\,\mathrm{d}\rho\,\mathrm{d}\omega$$
$$+ \int_{S^1}\int_I \frac{|\Phi_n(\omega) - x_0|}{\rho + 2\,|\Phi_n(\omega) - x_0|} (\partial_r \mathcal{M}f)(\Phi_n(\omega), \rho + |\Phi_n(\omega) - x_0|)\,\mathrm{d}\rho\,\mathrm{d}\omega\,. \quad (3.1)$$

Now let us denote the integrands of the two terms in this formula by $I_{1,n}\colon S^1 \times I \to \mathbb{R}$ and $I_{2,n}\colon S^1 \times I \to \mathbb{R}$, i.e.

$$I_{1,n}(\omega,\rho) := |\Phi_n(\omega) - x_0| \left(\partial_r^2 \mathcal{M}f\right)(\Phi_n(\omega), \rho + |\Phi_n(\omega) - x_0|) \ln|\rho|\,, \quad (3.2)$$
$$I_{2,n}(\omega,\rho) := \frac{|\Phi_n(\omega) - x_0|}{\rho + 2|\Phi_n(\omega) - x_0|} (\partial_r \mathcal{M}f)(\Phi_n(\omega), \rho + |\Phi_n(\omega) - x_0|)\,. \quad (3.3)$$

Since (3.1) holds for any $n \in \mathbb{N}$ and the left hand side is independent on n, we get

$$2\pi f(x) = \lim_{n\to\infty} \int_{S^1}\int_I I_{1,n}(\omega,\rho)\mathrm{d}\rho\,\mathrm{d}\omega + \lim_{n\to\infty} \int_{S^1}\int_I I_{2,n}(\omega,\rho)\mathrm{d}\rho\,\mathrm{d}\omega\,. \quad (3.4)$$

To apply the dominated convergence theorem, in the next Lemma we verify that $I_{1,n}$ and $I_{2,n}$ are uniformly bounded by some integrable functions.

Lemma 3.1. *For any $f \in C_c^\infty(\mathcal{P})$ there are constants $c_1, c_2 \in (0,\infty)$ such that for all $n \in \mathbb{N}$ the functions $I_{1,n}$, $I_{2,n}$ defined by (3.2), (3.3) satisfy the following:*

(a) $|I_{1,n}(\omega,\rho)| \le c_1 |\ln|\rho||$ *for all* $(\omega,\rho) \in S^1 \times I$.

(b) $\sup\{|I_{2,n}(\omega,\rho)| : (\omega,\rho) \in S^1 \times I\} \le c_2$.

Proof. (a) In order to proof the first item we have to show that the functions $(\omega,\rho) \mapsto |\Phi_n(\omega) - x_0| \left(\partial_r^2 \mathcal{M}f\right)(\Phi_n(\omega), \rho + |\Phi_n(\omega) - x_0|)$ are uniformly bounded. For that purpose we use that the circular means of a compactly supported smooth function and all its radial derivatives can be estimated by

$$\left|\partial_r^k \mathcal{M}f(x,r)\right| \le C_k \min\{r^{-1}, 1\} \quad \text{for all } (x,r) \in \mathbb{R}^2 \times (0,\infty), \tag{3.5}$$

where C_k are certain constants depending only on f. Application of (3.5) with $k=2$ shows

$$\begin{aligned} &|\Phi_n(\omega) - x_0| \left(\partial_r^2 \mathcal{M}f\right)(\Phi_n(\omega), \rho + |\Phi_n(\omega) - x_0|) \\ &\qquad \le C_2 |\Phi_n(\omega) - x_0| \min\left\{\frac{1}{\rho + |\Phi_n(\omega) - x_0|}, 1\right\}. \end{aligned} \tag{3.6}$$

As easily verified, the function $(d,\rho) \mapsto d \min\{1/(\rho+d), 1\}$ is bounded on $(0,\infty)^2$. This shows that the left hand side in (3.6) is indeed uniformly bounded by some constant and yields item (a).

(b) For the proof of the second item we apply (3.5) for $k=1$, which shows that there is a constant C_1 with

$$\begin{aligned} &\frac{|\Phi_n(\omega) - x_0|}{\rho + 2|\Phi_n(\omega) - x_0|} \partial_r \mathcal{M}f(\Phi_n(\omega), \rho + |\Phi_n(\omega) - x_0|) \\ &\qquad \le C_1 \frac{|\Phi_n(\omega) - x_0|}{\rho + 2|\Phi_n(\omega) - x_0|} \min\left\{\frac{1}{\rho + |\Phi_n(\omega) - x_0|}, 1\right\}. \end{aligned} \tag{3.7}$$

Because x_0 is contained in any elliptical domain $\mathcal{E}_n$ and $\Phi_n \to \Phi$, there exists some $\epsilon > 0$ such that $|\Phi_n(\omega) - x_0| \ge \epsilon$ uniformly for all $n \ge n_0$. Again using that $(d,\rho) \mapsto d \min\{1/(\rho+d), 1\}$ is bounded on $(0,\infty)^2$ shows that the right hand side in (3.7) is uniformly bounded, and this concludes the proof of (b). ∎

Now we proceed with the proof of Theorem 1.1. In view of Lemma 3.1, the dominated convergence theorem and Equation (3.4) imply

$$f(x) = \frac{1}{2\pi} \int_{S^1} \int_I \lim_{n\to\infty} I_{1,n}(\omega,\rho)\, \mathrm{d}\rho\, \mathrm{d}\omega + \frac{1}{2\pi} \int_{S^1} \int_I \lim_{n\to\infty} I_{2,n}(\omega,\rho)\, \mathrm{d}\rho\, \mathrm{d}\omega. \tag{3.8}$$

Because $\mathcal{M}f$ depends continuously on both arguments and Φ is the pointwise limit of Φ_n, we have

$$\lim_{n\to\infty} I_{1,n}(\omega,\rho) = |\Phi(\omega) - x_0| \left(\partial_r^2 \mathcal{M}f\right)(\Phi(\omega), \rho + |\Phi(\omega) - x_0|) \ln|\rho|, \tag{3.9}$$

$$\lim_{n\to\infty} I_{2,n}(\omega,\rho) = \frac{|\Phi(\omega)-x_0|}{\rho+2|\Phi(\omega)-x_0|}\left(\partial_r \mathcal{M}f\right)\left(\Phi(\omega),\rho+|\Phi(\omega)-x_0|\right). \tag{3.10}$$

Consequently $2\pi f(x)$ equals

$$\begin{aligned}\int_{S^1}\int_I |\Phi(\omega)-x_0|\left(\partial_r^2\mathcal{M}f\right)\left(\Phi(\omega),\rho+|\Phi(\omega)-x_0|\right)\cdot\ln|\rho|\,\mathrm{d}\rho\,\mathrm{d}\omega \\ + \int_{S^1}\int_I \frac{|\Phi(\omega)-x_0|}{\rho+2\,|\Phi(\omega)-x_0|}\left(\partial_r\mathcal{M}f\right)\left(\Phi(\omega),\rho+|\Phi(\omega)-x_0|\right)\,\mathrm{d}\rho\,\mathrm{d}\omega\,.\end{aligned}$$

According to Remark 2.2 this shows

$$f(x) = \frac{1}{\pi}\int_{\partial\mathcal{P}} \langle \nu_x, x_0-x\rangle \int_0^\infty \frac{\partial_r\mathcal{M}f(x,r)}{r^2-|x-x_0|^2}\,\mathrm{d}r\,\mathrm{d}s(x)\,.$$

Hence, we have verified the inversion formula (1.6).

3.2 Proof of Theorem 1.2

In [12, Section 4.1], it is shown that for every x_0 outside of the support of f, the following identity between the spherical means and the solution of the wave equation holds true:

$$\int_0^\infty \frac{(r\mathcal{M}f)(x,r)}{r^2-|x_0-x|^2}\,\mathrm{d}r = \int_{|x-x_0|}^\infty \frac{\mathcal{U}f(x,t)}{\sqrt{t^2-|x_0-x|^2}}\,\mathrm{d}t\,.$$

Together with two integrations by parts this yields

$$\begin{aligned}-\frac{1}{2}\int_0^\infty \log\left|r^2-|x_0-x|^2\right|\partial_r\mathcal{M}f(x,r)\,\mathrm{d}r \\ &= \frac{1}{2}\int_0^\infty \frac{d}{dr}\log\left|r^2-|x_0-x|^2\right|\mathcal{M}f(x,r)\,\mathrm{d}r \\ &= \int_0^\infty \frac{(r\mathcal{M}f)(x,r)}{r^2-|x_0-x|^2}\,\mathrm{d}r \\ &= \int_{|x-x_0|}^\infty \frac{\mathcal{U}f(x,t)}{\sqrt{t^2-|x_0-x|^2}}\,\mathrm{d}t \\ &= \int_{|x-x_0|}^\infty \frac{d}{dt}\sqrt{t^2-|x_0-x|^2}\left(t^{-1}\mathcal{U}f\right)(x,t)\,\mathrm{d}t \\ &= -\int_{|x-x_0|}^\infty \sqrt{t^2-|x_0-x|^2}\left(\partial_t t^{-1}\mathcal{U}\right)f(x,t)\,\mathrm{d}t\,.\end{aligned}$$

After applying the gradient operator with respect to x_0 this shows

$$(x_0-x)\int_0^\infty \frac{\partial_r\mathcal{M}f(x,r)}{r^2-|x_0-x|^2}\,\mathrm{d}r = (x_0-x)\int_{|x-x_0|}^\infty \frac{\left(\partial_t t^{-1}\mathcal{U}\right)f(x,t)}{\sqrt{t^2-|x_0-x|^2}}\,\mathrm{d}t\,.$$

The last displayed equation together with the reconstruction formula (1.6) for the spherical means yields the identity

$$f(x_0) = \frac{1}{\pi} \int_{\partial\mathcal{P}} \langle \nu_x, x_0 - x \rangle \int_0^\infty \frac{(\partial_r \mathcal{M} f)(x,r)}{r^2 - |x_0 - x|^2} \, \mathrm{d}r \mathrm{d}s(x)$$
$$= \frac{1}{\pi} \int_{\partial\mathcal{P}} \langle \nu_x, x_0 - x \rangle \int_{|x-x_0|}^\infty \frac{(\partial_t t^{-1} \mathcal{U} f)(x,t)}{\sqrt{t^2 - |x - x_0|^2}} \, \mathrm{d}t \mathrm{d}s(x) \,.$$

This is the desired reconstruction formula (1.7) for the wave boundary data.

4 Numerical results

The numerical realization of the formulas (1.6), (1.7) can be done as in [5, 8]. For illustration, we present the numerical results for the recovery from the wave data. We consider the function f given by the phantom presented in Figure 4. The same phantom was used for testing the numerical performance of the reconstruction formulas in [5, 12]. The support of the corresponding function f is included in the parabolic domain

$$\mathcal{P} = \left\{ (a,b) \in \mathbb{R}^2 \mid b > 0.6\, a^2 \, - 1 \right\}.$$

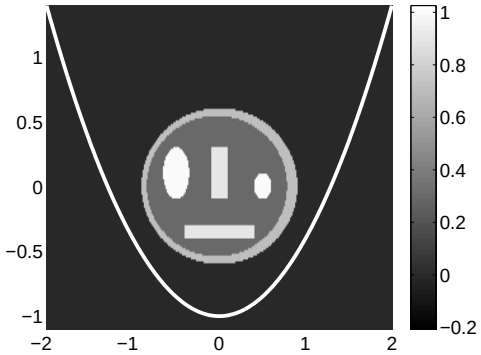

Figure 4: The phantom in the parabolic domain $\mathcal{P}$ that is used for the numerical results.

For the numerical realization of the formula (1.7) (which is (1.4) for the special case of a parabola), one first has to replace the integral over $\partial\mathcal{P}$ by the integral over a curve with finite length. We take the following integration curves (see Figure 5):

$$\Gamma_i = \left\{ (a,b) \in \mathbb{R}^2 \mid b = 0.6\, a^2 \, - 1, \; a \in [-a_i, a_i] \right\} \qquad \text{for } i = 1,2,3 \,,$$

with $a_1 = 2$, $a_2 = 4$, $a_3 = 6$, respectively. For comparison purpose, we also apply the inversion integrals to the closed curve $\bar{\Gamma}_i$ that is the union of the finite parabola Γ_i with the line between its endpoints, i.e.

$$\bar{\Gamma}_i = \Gamma_i \cup \left\{ (a,b) \in \mathbb{R}^2 \mid b = 0.6 a_i^2 \, - 1, \; a \in [-a_i, a_i] \right\}.$$

And we also take the ellipses

$$\Lambda_i = \left\{(a,b) \in \mathbb{R}^2 \mid a = r_{1,i}\cos(\theta),\ b = c_i + r_{2,i}\sin(\theta),\ \theta \in [-\pi,\pi)\right\},$$

with the parameters $\{c_i, r_{1,i}, r_{2,i},\ i = 1,2,3\}$ shown in Table 1 (left). Remember that for the ellipses, the formulas (1.3), (1.4) are analytically exact. The simulated wave data $\mathcal{U}f$ on the curves Γ_1, $\bar{\Gamma}_1$, Λ_1 are presented in Figure 6.

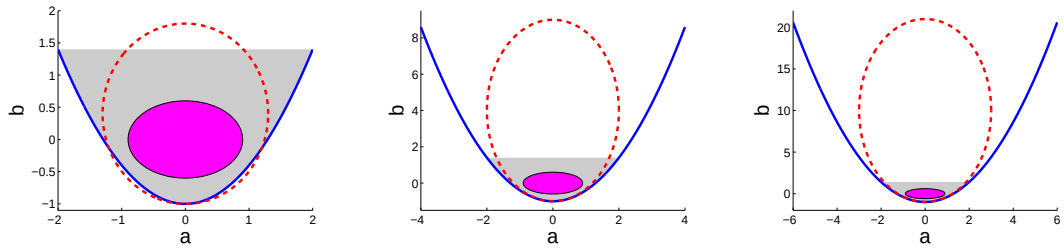

Figure 5: The considered integration curves (solid blue) Γ_i, $i = 1,2,3$ (from left to right). The ellipses Λ_i are shown as dashed red curves, and the support of the phantom f in Figure 4 is shown here in magenta. The reconstruction subdomain $\bar{\mathcal{P}}$ is shown in gray.

Table 1: Parameters of the ellipses Λ_i (left) and the numbers of the discretization points on the considered integration curves (right).

	1	2	3
c_i	0.4	4	10
$r_{1,i}$	1.3	2	3
$r_{2,i}$	1.4	5	11

	1	2	3
Γ_i	659	2166	4617
$\bar{\Gamma}_i$	1059	2966	5817
Λ_i	855	2317	4799

We consider the reconstructions $f_i(x)$, $\bar{f}_i(x)$, $\hat{f}_i(x)$ that are obtained by the numerical realization of the formula (1.7) where the integration curve $\partial\mathcal{P}$ is replaced by Γ_i, $\bar{\Gamma}_i$, Λ_i, correspondingly. These reconstructions on the reconstruction subdomain (the set where the inversion formula is evaluated)

$$\bar{\mathcal{P}} = \left\{(a,b) \in \mathbb{R}^2 \mid 0.6\,a^2 - 1 < b < 0.6\cdot 2^2 - 1,\ a \in (-2,2)\right\}$$

at the points $\left\{0.015(i,j) \mid (i,j)\right\} \in \mathbb{Z}^2\} \cap \bar{\mathcal{P}}$ are shown in Figure 7. The time step size for the inner integral in (1.7) is taken 0.01. The integration curves are discretized such that the distance between two consecutive points is in the interval $[0.0099, 0.0101]$. The numbers of the discretization points on the considered integration curves are presented in Table 1(right). In Table 2, one finds the scaled L_∞ and L_1 reconstruction errors that are defined as

$$L_\infty(f_i) = \frac{\max\limits_{x\in\bar{\mathcal{P}}} |\ f(x) - f_i(x)\ |}{\max\limits_{x\in\bar{\mathcal{P}}} |\ f(x)\ |}, \quad L_1(f_i) = \frac{\int_{\bar{\mathcal{P}}} |\ f(x) - f_i(x)\ |\,\mathrm{d}x}{\int_{\bar{\mathcal{P}}} |\ f(x)\ |\,\mathrm{d}x}.$$

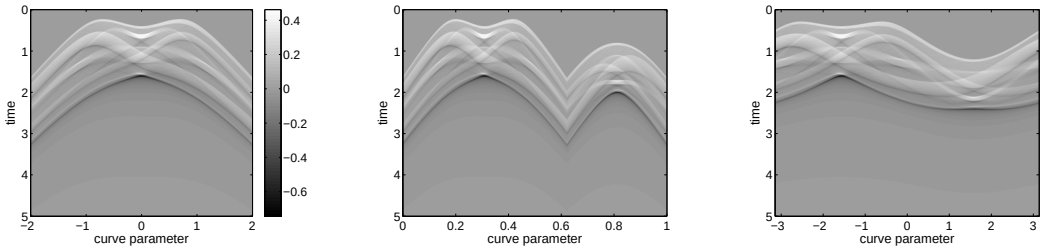

Figure 6: The simulated wave data $\mathcal{U}f$ on the integration curves Γ_1, $\bar{\Gamma}_1$, Λ_1 (from left to right). For the curve Γ_1 a is considered as the curve parameter. For the curve $\bar{\Gamma}_1$, the left top point of the parabola corresponds to the curve parameter 0; the parametrization is then goes along the parabola, and the endpoint corresponds to the curve parameter 1. For the ellipse Λ_1, we consider its parametrization with the parameter $\theta \in [-\pi, \pi)$.

One observes that the reconstruction errors for the ellipses Λ_i stay on the same level. Since the formula (1.3) is analytically exact for Λ_i, this error can be considered as the discretization error.

The reconstruction errors for the finite parabolas Γ_i are the highest, but it decreases as the length of Γ_i increases. It should be noted that the reconstruction problem in the case of the open curves Γ_i corresponds to the so-called limited view problem [18, 25, 26, 29]. For each reconstruction point inside the reconstruction subdomain $\bar{\mathcal{P}}$ there is a considerable set of directions for which the boundary wave data is missing, which is known to create reconstruction artefacts. On the contrary, for the closed curves $\bar{\Gamma}_i$, each reconstruction point in $\bar{\mathcal{P}}$ has the boundary wave data for all directions, but the reconstruction formulas (1.3) and (1.4) are not analytically exact on these curves. In [12], it has been shown that the reconstruction formulas (1.3) and (1.4) for the boundaries of convex bounded domains recover the unknown function modulo a smoothing integral operator. Thus, in addition to the discretization error, the reconstruction errors for $\bar{\Gamma}_i$ contains the error from an integral operator. As one can see in Table 2, this error component decreases as the length of $\bar{\Gamma}_i$ increases such that the reconstruction errors for $\bar{\Gamma}_3$ come very close to the discretization error.

Table 2: The scaled L_∞ and L_1 reconstruction errors of the numerical reconstructions.

	1	2	3
$L_\infty(f_i)$	0.6542	0.4991	0.4743
$L_\infty(\bar{f}_i)$	0.3614	0.3593	0.3522
$L_\infty(\hat{f}_i)$	0.3553	0.3566	0.3578

	1	2	3
$L_1(f_i)$	0.6219	0.4695	0.3882
$L_1(\bar{f}_i)$	0.2070	0.1335	0.1180
$L_1(\hat{f}_i)$	0.1088	0.1088	0.1088

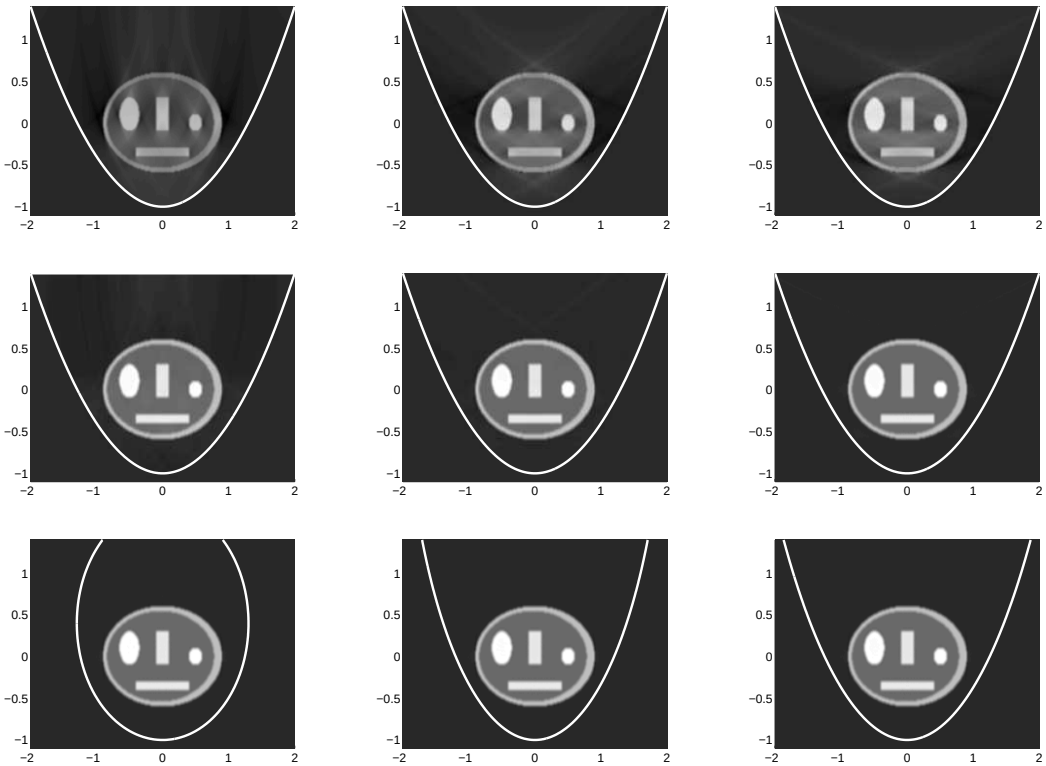

Figure 7: The numerical reconstructions f_i (top), $\bar{f}_i$ (middle), $\hat{f}_i$ (bottom), $i = 1, 2, 3$ (from left to right) on the reconstruction subdomain $\bar{\mathcal{P}}$. The gray scaling is as for the phantom in Figure 4 (left).

5 Concluding remarks

In this paper we derived explicit inversion formulas for recovering a function from special means or wave boundary data on the boundary of parabolic domains in $\mathbb{R}^2$; see Theorems 1.1 and 1.2. The same formulas were previously known to be applicable for spherical domains [5, 17, 27], half planes [3, 5, 20, 27] and elliptical domains [12, 21].

Our presented proof is based on the corresponding inversion formulas of [12] for elliptical domains and the fact that parabolas can be obtained as the pointwise limit of ellipsoids. Actually, the same proof can be made for any unbounded convex domains Ω such that for any $x_0 \in \Omega$, the following properties hold:

(a) The circular parameterization Φ of $\partial\Omega$ around x_0 is defined for almost all $\omega \in S^1$.

(b) There exists a sequence of elliptical domains $\mathcal{E}_n$ such that the conditions of Proposition 2.3 are valid, with the limit (2.5) being true for almost all $\omega \in S^1$.

In addition to the discussed parabolic domains, these two above properties are fulfilled also by strip domains, i.e. domains that are located between two parallel lines; for example a domain $\Omega = \big\{(a,b) \in \mathbb{R}^2 \mid 0 < b < 1\big\}$. The different elliptical approximations of the parabolic and strip domains are illustrated in Figure 8. Consequently, Theorems 1.1 and 1.2 also hold for such strip domains.

It is interesting to note that reconstruction formulas for data on the boundary of a strip domain can be also obtained from known formulas for the lines, or the hyperplanes in the multi-dimensional case [5, 4, 27, 3, 20]. For example, let us illustrate this simple observation for the corresponding formula $\mathcal{F}_{\text{str}}$ for the circular means data. Let Ω be a strip domain located between parallel lines $\partial\Omega_1$ and $\partial\Omega_2$. Note that $\partial\Omega = \partial\Omega_1 \cup \partial\Omega_2$. Further, let $\mathcal{F}_{\text{hyp}}$ be a reconstruction formula for the line (hyperplane). Then, for any $x_0 \in \Omega$, we have $f(x_0) = \mathcal{F}_{\text{hyp}}(\partial\Omega_1, \mathcal{M}f, x_0)$ and $f(x_0) = \mathcal{F}_{\text{hyp}}(\partial\Omega_2, \mathcal{M}f, x_0)$. Adding these two equations, we obtain a reconstruction formula for the boundary of the strip domain:

$$\begin{aligned} f(x_0) &= \frac{1}{2}\left(\mathcal{F}_{\text{hyp}}(\partial\Omega_1, \mathcal{M}f, x_0) + \mathcal{F}_{\text{hyp}}(\partial\Omega_2, \mathcal{M}f, x_0) \right) \\ &= \mathcal{F}_{\text{str}}(\partial\Omega, \mathcal{M}f, x_0). \end{aligned}$$

Notice, however, that the half-planes do not fulfil the above mentioned properties (a), (b) and therefore, the presented proofs of Theorems 1.1 and 1.2 can not be used for these domains.

Similar to the two dimensional case considered in this article one can derive inversion formulas for spherical means and wave boundary data on certain unbounded convex domains $\Omega \subset \mathbb{R}^d$ with $d > 2$. For that purpose one requires that the domain Ω satisfies conditions analogous to (a), (b) in higher dimensions and uses the inversion formulas of [13, 21] for elliptical domains in higher dimension. Elliptical cylinders and paraboloids are natural candidates for carrying out these generalizations. Such investigations are subject of future work.

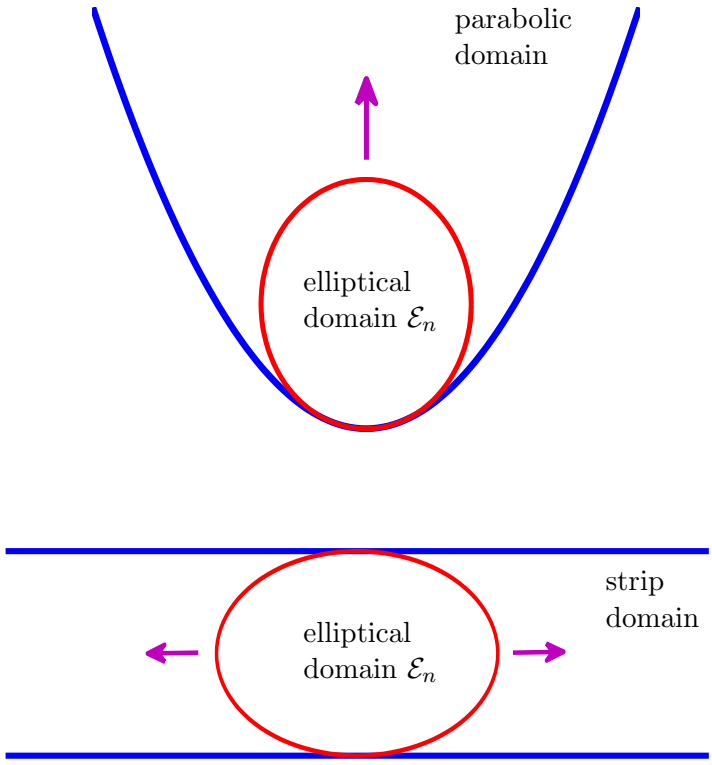

Figure 8: Comparison between the elliptical approximations of the parabolic (top) and strip (bottom) domains.

References

[1] L. E. Andersson. On the determination of a function from spherical averages. *SIAM J. Math. Anal.*, 19(1):214–232, 1988.

[2] M. Ansorg, F. Filbir, W. R. Madych, and R. Seyfried. Summability kernels for circular and spherical mean data. *Inverse Probl.*, 29:015002, 2013.

[3] A. Beltukov. Inversion of the spherical mean transform with sources on a hyperplane. Technical report, ArXiv e-prints, October 2009.

[4] A. L. Buhgeim and V. B. Kardakov. Solution of an inverse problem for an elastic wave equation by the method of spherical means. *Sibirsk. Mat. Z.*, 19(4):749–758, 1978.

[5] P. Burgholzer, J. Bauer-Marschallinger, H. Grün, M. Haltmeier, and G. Paltauf. Temporal back-projection algorithms for photoacoustic tomography with integrating line detectors. *Inverse Probl.*, 23(6):S65–S80, 2007.

[6] P. Burgholzer, G. J. Matt, M. Haltmeier, and G. Paltauf. Exact and approximate imaging methods for photoacoustic tomography using an arbitrary detection surface. *Physical Review E*, 75(4):046706, 2007.

[7] J. A. Fawcett. Inversion of n-dimensional spherical averages. *SIAM J. Appl. Math.*, 45(2):336–341, 1985.

[8] D. Finch, M. Haltmeier, and Rakesh. Inversion of spherical means and the wave equation in even dimensions. *SIAM J. Appl. Math.*, 68(2):392–412, 2007.

[9] D. Finch, S. Patch, and Rakesh. Determining a function from its mean values over a family of spheres. *SIAM J. Math. Anal.*, 35(5):1213–1240, 2004.

[10] M. Haltmeier. Frequency domain reconstruction for photo- and thermoacoustic tomography with line detectors. *Math. Models Methods Appl. Sci.*, 19(2):283–306, 2009.

[11] M. Haltmeier. A mollification approach for inverting the spherical mean Radon transform. *SIAM J. Appl. Math.*, 71(5):1637–1652, 2011.

[12] M. Haltmeier. Inversion of circular means and the wave equation on convex planar domains. *Comput. Math. Appl.*, 65(7):1025–1036, 2013.

[13] M. Haltmeier. Universal inversion formulas for recovering a function from spherical means. *SIAM J. Math. Anal.*, 41(1):214–232, 2014.

[14] M. Haltmeier, O. Scherzer, P. Burgholzer, R. Nuster, and G. Paltauf. Thermoacoustic tomography and the circular Radon transform: exact inversion formula. *Math. Models Methods Appl. Sci.*, 17(4):635–655, 2007.

[15] Y. Hristova, P. Kuchment, and L. Nguyen. Reconstruction and time reversal in thermoacoustic tomography in acoustically homogeneous and inhomogeneous media. *Inverse Probl.*, 24(5):055006 (25pp), 2008.

[16] P. Kuchment and L. A. Kunyansky. Mathematics of thermoacoustic and photoacoustic tomography. *European J. Appl. Math.*, 19:191–224, 2008.

[17] L. A. Kunyansky. Explicit inversion formulae for the spherical mean Radon transform. *Inverse Probl.*, 23(1):373–383, 2007.

[18] L. A. Kunyansky. Thermoacoustic tomography with detectors on an open curve: an efficient reconstruction algorithm. *Inverse Probl.*, 24(5):055021, 2008.

[19] L. A. Kunyansky. Reconstruction of a function from its spherical (circular) means with the centers lying on the surface of certain polygons and polyhedra. *Inverse Probl.*, 27(2):025012, 2011.

[20] E. K. Narayanan and Rakesh. Spherical means with centers on a hyperplane in even dimensions. *Inverse Probl.*, 26(3):035014, 2010.

[21] F. Natterer. Photo-acoustic inversion in convex domains. *Inverse Probl. Imaging*, 6(2):1–6, 2012.

[22] L. V. Nguyen. On a reconstruction formula for spherical radon transform: a microlocal analytic point of view. *Analysis and Mathematical Physics*, pages 1–22, 2013.

[23] S. J. Norton and M. Linzer. Ultrasonic reflectivity imaging in three dimensions: Exact inverse scattering solutions for plane, cylindrical and spherical apertures. *IEEE Trans. Biomed. Eng.*, 28(2):202–220, 1981.

[24] V. P. Palamodov. A uniform reconstruction formula in integral geometry. *Inverse Probl.*, 28(6):065014, 2012.

[25] G. Paltauf, R. Nuster, and P. Burgholzer. Weight factors for limited angle photoacoustic tomography. *Phys. Med. Biol.*, 54(11):3303, 2009.

[26] G. Paltauf, R. Nuster, M. Haltmeier, and P. Burgholzer. Experimental evaluation of reconstruction algorithms for limited view photoacoustic tomography with line detectors. *Inverse Probl.*, 23(6):S81–S94, 2007.

[27] M. Xu and L. V. Wang. Universal back-projection algorithm for photoacoustic computed tomography. *Physical Review E*, 71(1):0167061–0167067, 2005.

[28] M. Xu and L. V. Wang. Photoacoustic imaging in biomedicine. *Rev. Sci. Instruments*, 77(4):041101, 2006.

[29] Y. Xu, L. V. Wang, G. Ambartsoumian, and P. Kuchment. Reconstructions in limited-view thermoacoustic tomography. *Med. Phys.*, 31(4):724–733, 2004.

[30] Y. Xu, M. Xu, and L. V. Wang. Exact frequency-domain reconstruction for thermoacoustic tomography–II: Cylindrical geometry. *IEEE Trans. Med. Imag.*, 21:829–833, 2002.